Available online at www.sciencedirect.com
ScienceDirect
Polymer 48 (2007) 1667–1678
polymer
www.elsevier.com/locate/polymer

Structure and conductivity of multi-walled carbon nanotube/poly(3-hexylthiophene) composite films

Anthony W. Musumeci [a], Glaura G. Silva [b,*], Jiang-Wen Liu [a], Wayde N. Martens [a], Eric R. Waclawik [a]

[a] *Inorganic materials Research Program, School of Physical and Chemical Sciences, Queensland University of Technology, GPO Box 2434, Brisbane, Queensland 4001, Australia*

[b] *Departmento de Química, Universidade Federal de Minas Gerais, Pampulha, C.P. 702, Belo Horizonte 31270-901, Minas Gerais, Brazil*

Received 9 November 2006; received in revised form 9 January 2007; accepted 10 January 2007
Available online 20 January 2007

Abstract

This work reports a structure–property investigation of a conjugated polymer nanocomposite with enhanced conductivity. Regioregular poly(3-hexylthiophene) (rrP3HT) was used to prepare composites with thin, short, multi-walled carbon nanotube (MWNT) addition over a wide range of concentrations. Scanning and transmission electron microscopies demonstrated an excellent dispersion and good wetting properties within the carbon nanotube composites. Coated MWNTs showed superstructures of P3HT self-organized on nanotube surfaces. Changes in the long range order and on the self-ordered mesophase of the bulk material were investigated by infrared and Raman spectroscopies, differential scanning calorimetry and X-ray diffraction. Interplay between charge transport through the semiconducting polymer and carbon nanotube network increased the composite's conductivity after percolation to values close to 10^{-2} S cm^{-1}.

Keywords: Multi-walled carbon nanotubes; Regioregular poly(3-hexylthiophene); Conductivity

1. Introduction

Conjugated polymer materials are of interest to both scientists and engineers alike because they can be prepared with similar electrical and optical properties to semiconductors or even metals, while still retaining the attractive mechanical properties and processing advantages of polymers [1]. Not long after their discovery by Shirakawa et al., conjugated or conductive polymeric materials were quickly identified as promising candidates for use as the active component of a variety of electronic devices, such as low-cost alternatives to conventional light-emitting diodes (LEDs), photovoltaic cells and even disposable electronic chips [2,3]. Poly(alkylthiophene)s such as poly(3-hexylthiophene) (P3HT) have been the focus of great attention due to a combination of their relatively high chemical stability in ambient conditions, their high conductivity and the fact that the electronic band gap of these materials generally falls within the visible region of the electromagnetic spectrum.

Recently interest has been focused on the preparation of solution processed thin films of regioregular poly(3-hexylthiophene) (rrP3HT) [4–12], due to its great potential for a variety of applications as, for instance, field-effect transistors [4–6] and photovoltaic cells [7,8]. It is now well known that the optoelectronic properties of P3HT films are highly sensitive to microstructure and film morphology which depend on many materials and processing variables. These variables, e.g. solvent type, temperature, film-casting technique, P3HT average molar mass and polydispersity, to name a few, are often linked together in non-trivial ways. The microscopic structure of bulk rrP3HT prepared from solution has been investigated in great detail for more than 15 years [13–20]. Certainly, when tailoring the electronic properties of P3HT materials, the first important consideration is to determine the effect of regioregularity and

* Corresponding author. Tel.: +55 31 3499 5768; fax: +55 31 3499 5700.
E-mail address: glaura@qui.ufmg.br (G.G. Silva).

0032-3861/$ - see front matter © 2007 Elsevier Ltd. All rights reserved.
doi:10.1016/j.polymer.2007.01.027

molar mass of the polymer on the final material's quality and properties [9,10,20]. Solvatochromic and thermochromic behaviours have also been recognized [13,14,21]. A rod-to-coil conformational change occurs when a P3HT sample is dispersed in a good solvent or heated above thermal transitions [21]. The nature of crystalline, amorphous and mesophase properties does not appear to be completely understood up to now. Two crystalline phases and a liquid crystalline mesophase have been proposed to explain the results of differential scanning calorimetry (DSC) and X-ray diffraction (XRD) [11–13,15,18,19]. In the context of thin films, fibrillar morphology induces important enhancements in properties such as charge carrier transport [4,5].

Carbon nanotubes (NTs) provide a tailored structure to interact with conjugated polymers by means of π–π electronic interactions. A recent review on conductive nanocomposites [22] points to the fact that NTs have good potential to enhance the optoelectronic properties of conjugated polymers. It has been shown that when fillers have an aspect ratio of 10^3 (a possible value obtainable for the case of single-walled carbon nanotubes, SWNTs) the expected percolation threshold is much less than 1 wt% [23]. In the case of composites formed with multi-walled carbon nanotubes (MWNTs), spectroscopic and microscopic investigations of conjugated polymer/MWNT systems based on derivatives of poly(phenylenevinylene) [24] have identified considerable polymer–MWNT interaction and strong evidence of polymer wrapping of the nanotube's outermost basal-plane sidewalls. Kilbride et al. [25] reported the conductivity behaviour of the same system with a percolation threshold of 0.055 wt% of MWNT but only very low DC conductivity of 1.4×10^{-7} S cm^{-1} for a composite containing 4.3 wt% MWNTs. Similar low conductivity value of approximately 5×10^{-7} S cm^{-1} was observed for a composite of poly(3-octylthiophene) containing 5 wt% SWNT [26], however, in this case the critical mass for percolation of 4 wt% was probably associated to SWNT bundling.

Percolation is a volumetric phenomenon; however, as the density of carbon nanotube samples is not always reported, it is necessary to compare the results of conductivity studies by using concentrations expressed in terms of weight percent [27]. The conductivity of isotropic PMMA/SWNT studied by Du et al. [28] exhibited a percolation threshold of 0.365 wt% and conductivity of 3.5×10^{-4} S cm^{-1} for a 2 wt% SWNT composite. This work also reported an interesting dependence of conductivity with alignment for samples prepared by melt fiber spinning method [28]. Koerner et al. [29] reported percolation threshold of 0.85 wt% for a thermoplastic polyurethane/MWNT composite. In the case of polystyrene and polycarbonate/SWNT composites investigated by Ramasubramaniam et al. [30], values of 0.05 and 0.1 wt% for critical mass of SWNTs were obtained, respectively. Several studies have reported low percolation thresholds for epoxy/NT composites, below 0.1 wt% [31–34], while Barrau et al. [35] measured a percolation threshold of 0.3 wt% for epoxy/NT. Park et al. [36] and McLachlan et al. [37] obtained a percolation threshold of 0.05 wt% for polyimide/SWNT. The semicrystalline polyethylene oxide (PEO) was investigated by Chatterjee et al. [38] as matrix for SWNT addition and electrical percolation was obtained at 0.03 wt% NT. In the case of melt processed polyethylene/NT, higher critical masses of 4 wt% [39] and 7.5 wt% [40] were observed, but these values are associated with agglomeration of carbon nanotubes in melt processed composites. The same behaviour was observed for melt processed polycarbonate/MWNT with a percolation threshold between 1 and 1.5 wt% nanotubes [41]. Several of the above mentioned works on insulating polymer/NT composites had conductivities close to 10^{-4} S cm^{-1} on the plateau near and after percolation, at approximately 2 wt% [28,33,35,38,40,41]. These works investigated very different materials and processing conditions, yet conductivity just after percolation seems to converge to the value 10^{-4} S cm^{-1} on the plateau after percolation, at variable concentration, some other NT composites have conductivity values that range from 10^{-6} to 10^{-2} S cm^{-1} [26,30–32,34,36,37,39] on the plateau.

Two problems concerning poly(3-hexylthiophene)–carbon nanotube composites have been addressed in this work: firstly the nature of polymer–NT interaction, wrapping or not and phase structure of the bulk materials were investigated; secondly the conductivity trend as a function of nanotube concentration was measured and the applicability of percolation models for this conjugated polymer–NT system was evaluated.

2. Experimental

2.1. Composite preparation

Short, thin, multi-walled carbon nanotubes purchased from Nanocyl S.A. (>95% carbon purity, ~10 nm diameter, <1 μm length) were used in all composite films without further purification. The MWNTs were dispersed at a ratio of 1 mg MWNT:100 mL of chloroform (UniVar, AR reagent) in an ultrasonic bath (output: 50 W) for 6 h to yield a stable dispersion with minimal nanotube aggregation. Typically, 40 mg of regioregular poly(3-hexylthiophene) (American Dye Source, $M_r = 28\,000$ g/mol) was dissolved in a minimum amount of chloroform. A given volume of nanotube dispersion was added to the concentrated polymeric solution to yield the desired loading of MWNTs in rrP3HT (from 0.01 to 30 wt%). The composite chloroform solution was then sonicated for further 30 min before being added to an excess amount of methanol (UniVar, AR reagent, typically 400–700 mL) to induce polymer aggregation with simultaneous precipitation of the MWNTs through polymer–NT non-covalent interactions [42,43]. The excess solvent was then rotary evaporated from the composite solution to yield a concentrated polymer–nanotube dispersion in methanol. Remaining methanol was then evaporated in a petri dish on a hotplate at low temperature to yield a thin, well dispersed nanotube/polymer composite.

The resulting composites were analysed using transmission and scanning electron microscopies (TEM and SEM), Raman and infrared spectroscopies, differential scanning calorimetry (DSC) and X-ray diffraction (XRD) to determine

morphological, compositional and phase characteristics. The conductivity of the composites was measured using DC-resistance and AC-impedance techniques.

2.2. Instrumentation

Scanning electron microscopic (SEM) analysis of composite film cross sections was achieved by freezing the thin composite film in liquid nitrogen and then fracturing the composite and mounting vertically on a drop of silver paste. The neat MWNT sample was imaged by drop casting a dilute MWNT dispersion in chloroform (1 mg/100 mL) onto a polished silicon wafer. The samples were then coated with a thin layer of gold to reduce charging during analysis. Secondary electron images were obtained using an FEI Quanta 200 environmental scanning electron microscope. Accelerating voltages of 25–30 kV and spot size settings of 2–2.5 were used for carbon nanotube samples whilst accelerating voltages not exceeding 15 kV and a spot size of 3–3.5 were required for the polymeric composite material to avoid sample degradation.

Transmission electron microscopic (TEM) analysis was carried out with a JEOL TEM-2010 with an acceleration voltage of 200 kV. Samples for TEM studies were prepared by sonication of diluted dispersions in methanol and drop casting on a carbon-coated copper grid.

For Raman spectroscopy a small amount of sample was placed on a polished metal surface on the stage of a Leica microscope, which was equipped with 10× and 50× short and long working distance objective lenses. The microscope was part of a Renishaw 1000 microscope system that also included a monochromator, RSSF notch filter system and charge coupled detector. Raman spectra were excited by a Renishaw near-infrared diode laser, emitting at 785 nm, and recorded through Wire2 software. The 785 nm laser was the preferred excitation wavelength for the composite samples due to the reduced fluorescence and more stable background achievable. The samples were analysed at an intensity of 10–0.05% laser power (13.5–0.0675 mW at the sample surface, respectively) with a slight defocusing of the laser beam in order to avoid laser-induced sample degradation. Spectra were typically taken from 2000 to 100 cm^{-1} in the Stokes region and were calibrated against the 520.5 cm^{-1} line of a silicon wafer. The signal to noise ratio was enhanced by repeated acquisitions, typically through 4 × 60 s scans. Spectroscopic manipulations such as baseline adjustment, smoothing and normalisation were performed using the GRAMS spectracalc software package (Galactic Industries Corporation, NH, USA). Band component analysis was undertaken using the Jandel 'Peakfit' software package. Band fitting was done using a Gauss–Lorentz cross-product function with the minimum number of component bands used for the fitting process. The Gauss–Lorentz ratio was maintained at values greater than 0.7 and fitting was undertaken until reproducible results were obtained with squared correlations greater than 0.995.

Infrared spectra were obtained using a Nicolet Nexus 870 FTIR spectrometer with a smart endurance single-bounce diamond attenuated total reflectance (ATR) cell. Spectra over the range 4000–525 cm^{-1} were obtained by the co-addition of 64 scans operated at a resolution of 4 cm^{-1} and a mirror velocity of 0.6329 cm/s. Spectral manipulations such as baseline adjustment, smoothing and band fitting were performed using GRAMS® and Jandel 'Peakfit' software packages.

Samples were prepared for X-ray diffraction by heating the polymeric composite on hotplate to ~200 °C and compressing the material into a thin film on a low background silicon wafer. The silicon wafer was then mounted on customised aluminium sample holders to allow X-rays to be detected at small scattering angles. X-ray diffraction patterns were collected using a Philips X'pert wide angle X-ray diffractometer, operating in step scan mode, with Cu Kα radiation (1.54052 Å). Patterns were collected in the range 4–30° 2θ with a step size of 0.02° and a rate of 8 s per step (overall scan time ~3 h). The instrument was run in parallel beam mode with an incident angle of 4.5° and the sample spun at 60 rpm during analysis. Crystallite size calculations were made in the PANalytical-X-Pert Highscore software package. Diffraction patterns were firstly baseline corrected before profile-fitting to the first reflection was preformed. The full-width at half-maximum (FWHM) height of the peak and peak position was then obtained from the fit to the first reflection and the polymer crystallite size was estimated through the Scherrer Calculator tool.

Differential scanning calorimetric measurements were carried out with a Q100 TA Instruments DSC which was calibrated with an indium standard. Cyclic runs between room temperature and 300 °C were performed at 10 °C/min with approximately 3 mg samples placed in aluminium crucibles under nitrogen atmosphere. First and second heating runs, as well the cooling runs, were analysed.

AC-impedance measurements were carried out at a range of temperatures from 150 to 25 °C. AC-impedance measurements were carried out using a Princeton Applied Research, Model 273A Potentiostat coupled with a Lock in amplifier (Model No. 5210). Impedance data were acquired through PowerSuite Software, in the frequency range 0.12–5 Hz with an AC amplitude of 40 mV. DC current measurements were carried out on a Fluke 45 Digital multimeter. A symmetrical cell of two stainless steel electrodes was designed to sandwich a polymer composite film under pressure in the middle. Samples of thickness in the range 100–250 μm were previously measurement annealed for 16 h at 150 °C under pressure between the electrodes to assure good electric contact.

3. Results and discussion

Analysis of scanning electron microscopic (SEM) and transmission electron microscopic images of the MWNT samples confirmed the distribution of length, l, and diameter, d, in the material, $\overline{l} \approx (0.94 \pm 0.22)$ μm, $\overline{d} = (10.3 \pm 1.2)$ nm, see Fig. 1. The length was assessed from SEM pictures by measuring thirteen isolated and uncurled nanotubes in low concentrated regions of the sample. The diameter was evaluated from analysis of 55 nanotubes; an estimated average number

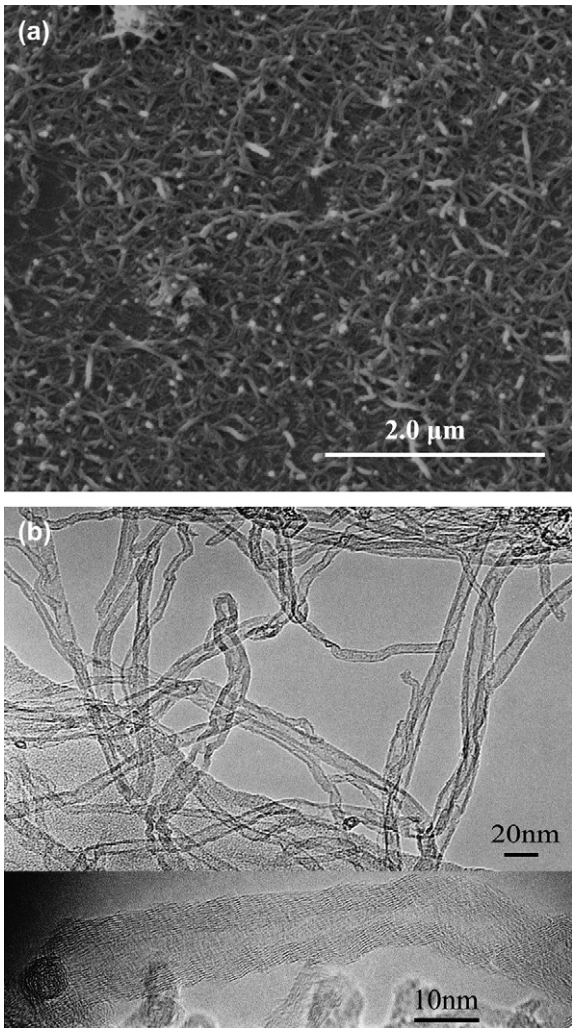

Fig. 1. (a) SEM and (b) TEM images of short, thin MWNT.

of 8 ± 2 walls per MWNT was obtained from observation of 15 nanotubes in high-resolution TEM images. The manufacturers stated carbon purity of >95% and metal oxide impurity of <5% were confirmed by thermogravimetric analysis (not shown).

Typical cryo-fractured surface images are presented in Fig. 2a, where the P3HT and composites were prepared by addition of the poor solvent methanol to chloroform-dispersed solutions. In the case of a pure P3HT film initially a morphology of globular aggregates was observed. After thermal annealing, the films became more compact, as observed in Fig. 2a, and the film surfaces displayed a shiny metallic lustre to the naked eye. The pure polymer precipitated easily from solution with methanol addition, whereas the composite dispersions were stable in solution for a long period of time or did not precipitate at all. This observation is a first indication of a strong interaction between NT and polymer that disturbed the polymer self-organization, inducing a new structural arrangement. It thus appears that the polymer–NT self-assembly in a poor solvent minimised the surface area of the aggregates exposed to solvent, hindering easy precipitation. Nevertheless, all dispersions possessed the typical magenta colour characteristic of polymer molecule rod conformation in a poor solvent [21].

The SEM images in Fig. 2b and c displayed the typical morphology of the very good dispersion of the MWNT in the polymer matrix for the composites in this work. It was observed that isolated MWNTs embedded in polymer matrix were present over the full range of nanocomposite concentrations studied. Considering the individual MWNT dimensions evaluated by SEM and TEM it was concluded that nanocomposites with a filler aspect ratio of 91 ± 24 were produced.

In order to look for more information about the polymer–NT interface, TEM images of drop coated, much diluted dispersions of 4 and 17 wt% composites were obtained. Typical images are shown in Fig. 2d–f. It is possible to observe fully coated and partially coated MWNTs because of the high dilution employed to prepare the samples for TEM. After a careful examination of 20 TEM images no special ordered polymer wrapping structure or crystal growth was discerned in the P3HT/MWNT system. This is unlike the ordered helical-wrapping structures observed by McCarthy et al. [24] for PmPV/MWNT. There was, however, a distinct tendency for polymer chain alignment (of rod segments) with the NT main axis, as can be observed in Fig. 2f and specifically in Fig. 3.

Fig. 3 shows coated MWNTs with regions of aligned rod-like self-assembly of P3HT chains. This interpretation is supported by observations made using scanning tunnelling microscopy (STM) of P3AT self-organization in strands on highly oriented pyrolytic graphite (HOPG) [44–46]. The alkyl side chains organize in a planar interdigitated fashion along the three main graphite axes with the conjugated backbones orientated perpendicular to them in highly ordered lamellae.

FTIR spectra of P3HT and composites are presented in Fig. 4. According to Furukawa et al. [47] and Trznadel et al. [20] the ratio between the intensity of the antisymmetric C=C stretching peak (mode at 1509 cm^{-1}) and the intensity of the symmetric stretching peak (mode at 1456 cm^{-1}) can be used to probe the average conjugation length of P3HT. Fig. 4 shows an inset with the trend in the calculated ratio that is with increasing MWNT content an increase of conjugation length is observed. This is a very interesting result which corroborates the TEM evidence for alignment of polymer segments on the NT surface. Considering that TEM image analysis of diluted composite films was limited to a small number of P3HT layers deposited upon the NT surface, the result of FTIR for the bulk composite films, on the other hand, indicates that the P3HT interfacial arrangement on the MWNT filler has consequences on the structure of the bulk material as a whole.

The Raman spectra of pure P3HT and MWNTs as well as MWNT/P3HT composites are presented in Fig. 5. The Raman spectrum of the neat MWNTs shows two broad peaks at 1306 and 1600 cm^{-1} which are attributed to the D and G-bands, respectively, commonly observed in an MWNT spectrum [40,48]. The native poly(3-hexylthiophene) spectrum is identical to previous results for rrP3HT, it features all vibrational frequencies expected for the conjugated polymer [49].

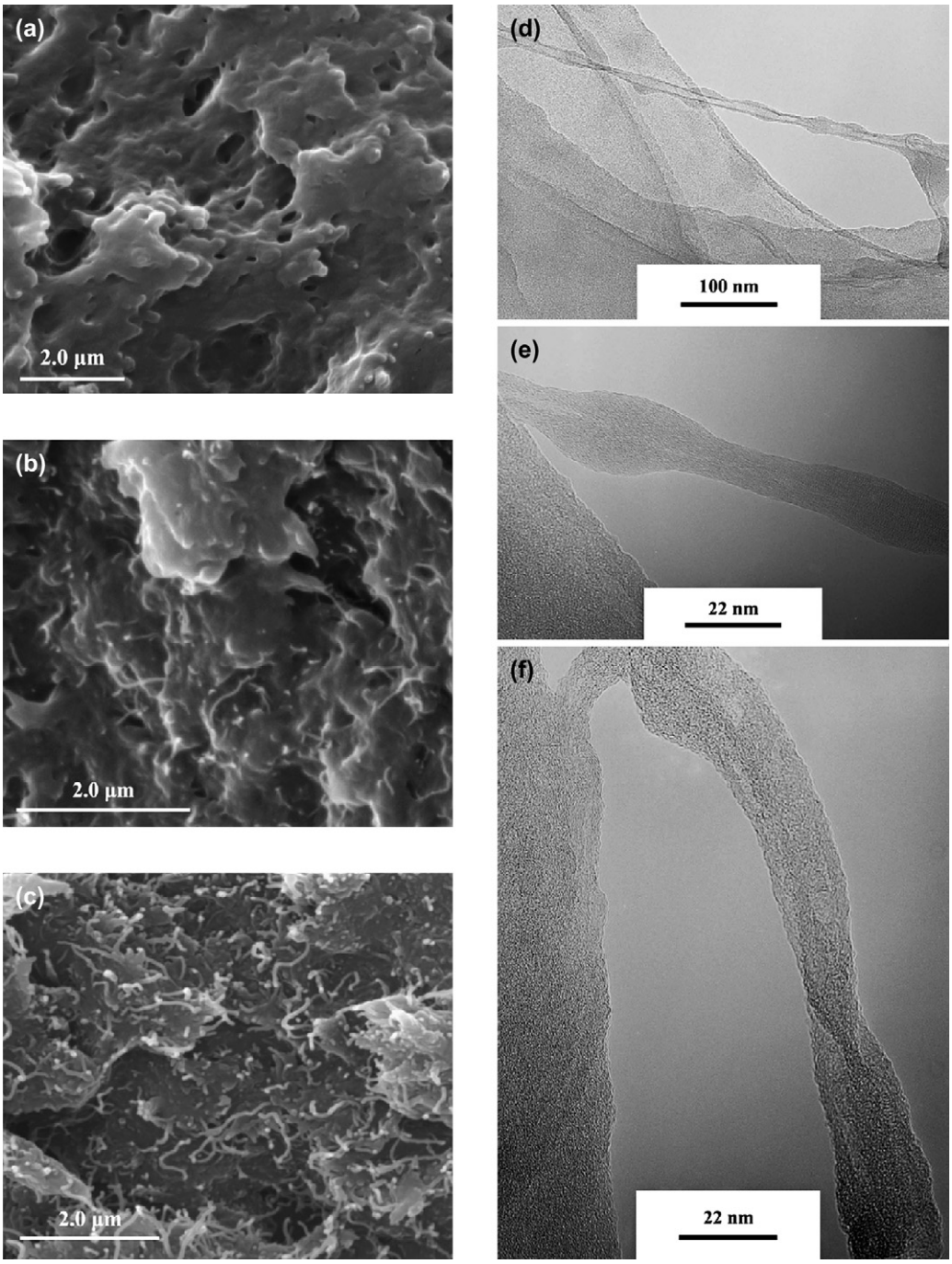

Fig. 2. SEM images of cryo-fractured surfaces of (a) P3HT and P3HT/MWNT composite films with (b) 1 wt% and (c) 17 wt% of MWNT. (d)–(f) TEM images of a drop coated from methanol sample of 4 wt% MWNT composite.

Interestingly an upshift of the carbon nanotube peaks of 10–15 cm^{-1} was observed in all composite samples. We have introduced the spectrum for a very concentrated sample, 55 wt% MWNT, in order to clearly show the displacement of the peaks. The observed upshift in the Raman signal in both the G and D-band frequencies is a direct consequence of an increase in the carbon nanotube C–C bond strength. Two possible explanations to the observed shift are detailed. Wise et al. [50] have reported the effect of electron donor–acceptor type charge addition to SWNTs with respect to shifts in characteristic Raman active vibrational modes. Specifically, removing charge from an SWNT results in an upshift in the G-band. Wise et al. [50] observed a downshift in the Raman D-band which was attributed to additional electron density in the SWNT's antibonding orbitals from charge injection causing a weakened average C–C bond length [50]. Thus, based on these considerations and the observed upshift in the MWNT–polymer matrix, it could be proposed that the MWNTs donate electronic charge to the polymer matrix.

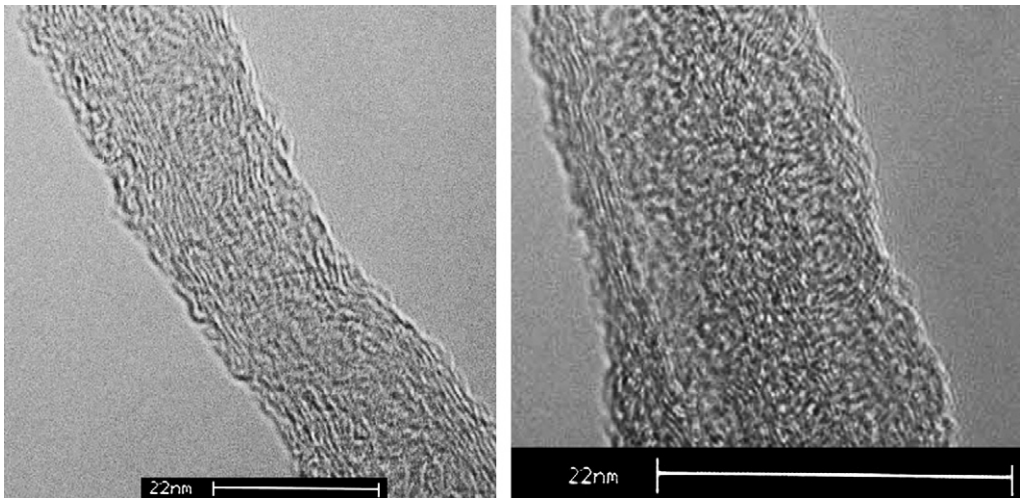

Fig. 3. TEM images of coated MWNT by P3HT; from 4 wt% dispersion in methanol.

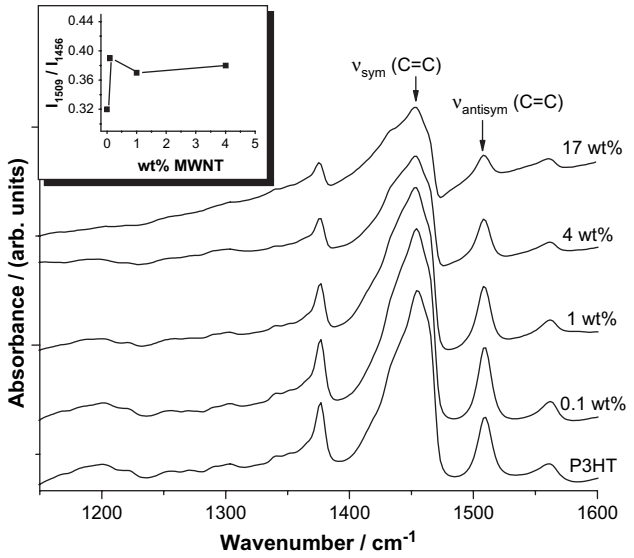

Fig. 4. FTIR spectra of P3HT and composites. Inset: relative intensity of C=C antisymmetric to symmetric stretching indicating an increase in conjugation length. The uneven baseline, observed for the 17 wt% MWNT composite, caused by the sample strongly absorbing incident radiation, prevents the evaluation of the ratio of relative intensities given in the inset for other compositions.

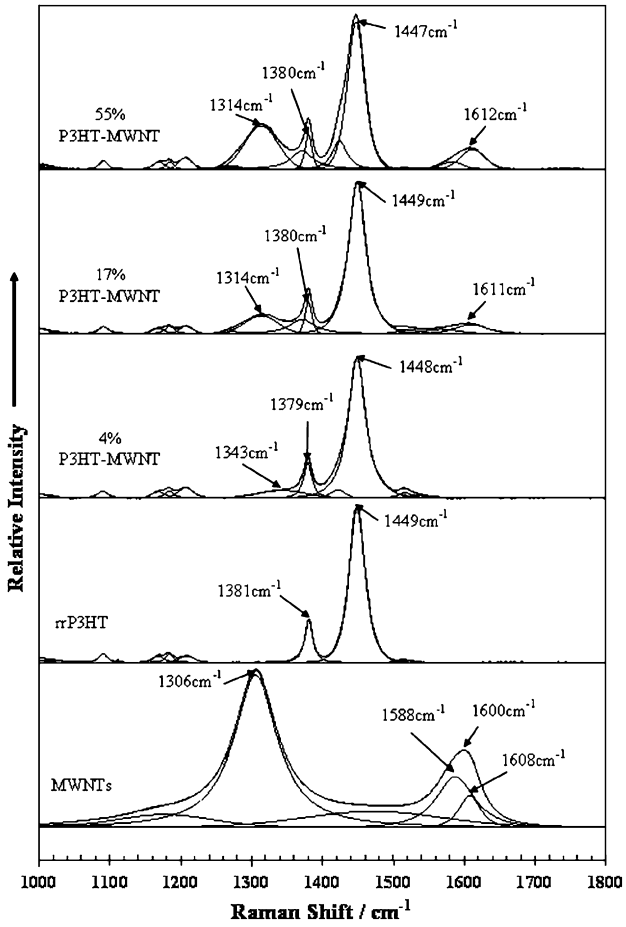

Fig. 5. Raman spectra of pure MWNT and P3HT as well as MWNT/P3HT composites of various compositions.

Otherwise, in a recent report by Baskaran and co-workers [48] concerning interactions between poly(butadiene)/MWNT composites, a similar upshift of 10–15 cm^{-1} was observed in the Raman spectra. The reported upshift was larger towards higher concentrations of poly(butadiene) in the composite material and attributed to an effect of the increased probability of enhanced coverage of the MWNTs surface with polymer, this in turn affects the freedom of C–C vibration on the graphene plane due to CH–π interactions. Thus, they concluded that CH–π interactions observed between nanotube and polymer are stronger than that of the π–π interactions observed between nanotube bundles, resulting in a restriction of the C–C bond vibrations and a corresponding upshift of the Raman signal. A 17 cm^{-1} upshift in G-band Raman signal of MWNTs embedded in melt-blended polyethylene/MWNT composites and the evolution of a shoulder to this peak have also been observed [40], where the changes were attributed to compressive forces exerted on the MWNTs by PE chains following intercalation into MWNT bundles. Considering

Table 1
DSC (10 °C/min) and X-ray diffraction results for P3HT and P3HT/MWNT composites

	First heating run		Second heating run		Second cooling run		XRD
	T_m^1 (°C)	ΔH^1 (J g^{-1})	T_m^2 (°C)	ΔH^2 (J g^{-1})	T_c (°C)	ΔH_c (J g^{-1})	Crystallite size (nm)
0	218 and 230	14	215 and 230	13	174	14	37.2
0.1	222	9.6	218 and 230	8.2	185	10	35.7
1	223	19	223	13	176	12	37.0
4	214	12	220	11	181	12	32.1
17	210	8.6	215	8.3	180	7.9	28.9

Accuracy: $T_m \pm 1$ °C and $\Delta H \pm 1$ J g^{-1}.

this behaviour is common to solution processed and melt extruded nanocomposite systems, conjugated, branched and linear alkyl-chain type polymers, the proposed compression-induced effect on MWNT Raman G-band position appears to be consistent with the results obtained for rrP3HT/MWNT composites.

P3HT and P3HT/MWNT composites' bulk structures were investigated by DSC and X-ray diffraction. The thermal transitions of poly(alkylthiophenes) have been intensively studied by these techniques [11–19]. For regioregular P3AT it has been proposed that the semicrystalline structure can show two types of crystals, one of them is interdigitated [51,52]. Side chain crystallization and the presence of a nematic mesophase in the liquid have also been proposed to occur based on different methods, materials and measurement conditions [12,13,15,18,19,51,52]. Table 1 shows a summary of DSC results taken under cyclic runs at 10 °C/min. A very low heat of melting is obtained for P3HT which is consistent with partial crystallinity and nematic mesophase in liquid. Fig. 6 shows DSC curves for the second heating run. The first important observation is that P3HT and 0.1 wt% MWNT composite present two overlapped thermal events in the melting region. Causin et al. [52] have assigned a similar decoupled endotherm for P3BT to a crystal–nematic transition followed by isotropization. However, there is evidence for persistence of the liquid crystal mesophase in P3HT at temperatures as high as 250 °C [12]. Winokur et al. [13] have also reported the observation of the nematic phase at high temperatures even with a non-regioregular sample. Upon cooling, the DSC measurements did not show two peaks, only one crystallization peak with approximately the same heat involved on melting (see Table 1). Therefore, it is proposed that the two overlapped transitions for P3HT and 0.1 wt% composite observed in our experimental conditions are related to two different crystals, one probably interdigitated [51], which is formed with a slow kinetic during the thermal treatment associated to the cyclic DSC runs. Also, a related work assumed the existence of two crystal structures, one interdigitated, for P3HT and its nanocomposites with montmorillonite clay [53].

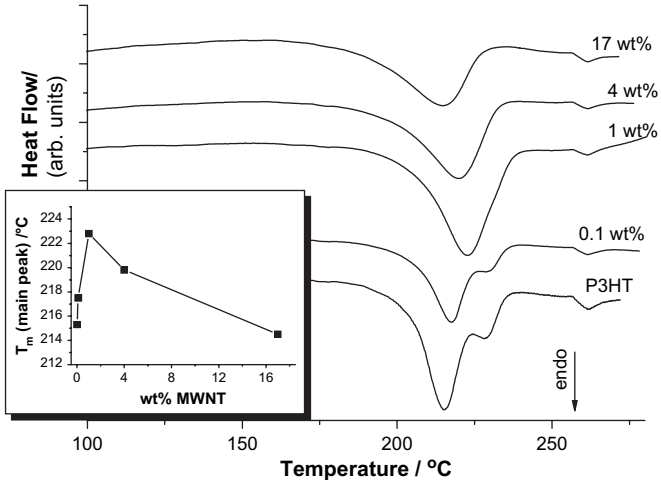

Fig. 6. DSC curves of second heating run and melting temperature (inset) of the main peak for P3HT and MWNT/P3HT composites at various concentrations indicated in the figure.

For the composites with 1 wt% of MWNT and higher MWNT concentrations, the crystal–mesophase transition is characterized by one peak only. For 1 wt% MWNT sample, an increase of transition temperature and heat of transition was observed (see Fig. 6 inset and Table 1), and for the higher MWNT-content composites the crystal structures appear to be less stable and less concentrated. The result of decrease in crystallinity with carbon nanotube addition of 4 wt%, for instance, is again opposite in behaviour compared to the results reported by Ryan et al. [54], for up to 5 wt% PmPV/MWNT. They observed a nucleating effect upon the polymer crystallinity that was attributed to carbon nanotube inclusion in the host. On the other hand, Chatterjee et al. [38] observed a strong decrease of crystallinity in PEO by addition of SWNT in a low concentration range of up to 0.2 wt% SWNT. Also, McNally et al. [40] observed decrease of crystallinity in series of PE/MWNT composites. Therefore, it seems that the effect of carbon nanotubes in polymer crystallinity is specific for each pair of components in the systems – nanotube and polymer – and the range of compositions studied.

It is interesting to note that the 1 wt% MWNT composite actually shows increase of melting temperature and heat of fusion in relation to the 0.1 wt% material. This behaviour can be ascribed to the influence of nanotubes increasing the order of the crystalline structure in a range of intermediary compositions. Considering that, when deposited on HOPG, monolayers of P3AT self-organize in interdigitated mesophases [44–46], this can be also the case for P3HT/MWNT.

X-ray diffraction patterns obtained at room temperature are presented in Fig. 7a. The scattering peaks at 5.2, 10.5 and 15.8 2θ arise from the first, second and third order reflections from the large length d-spacing (16.8 Å) for P3HT [15,55] and correspond to the in-plane interchain distance a (see Fig. 7b). In

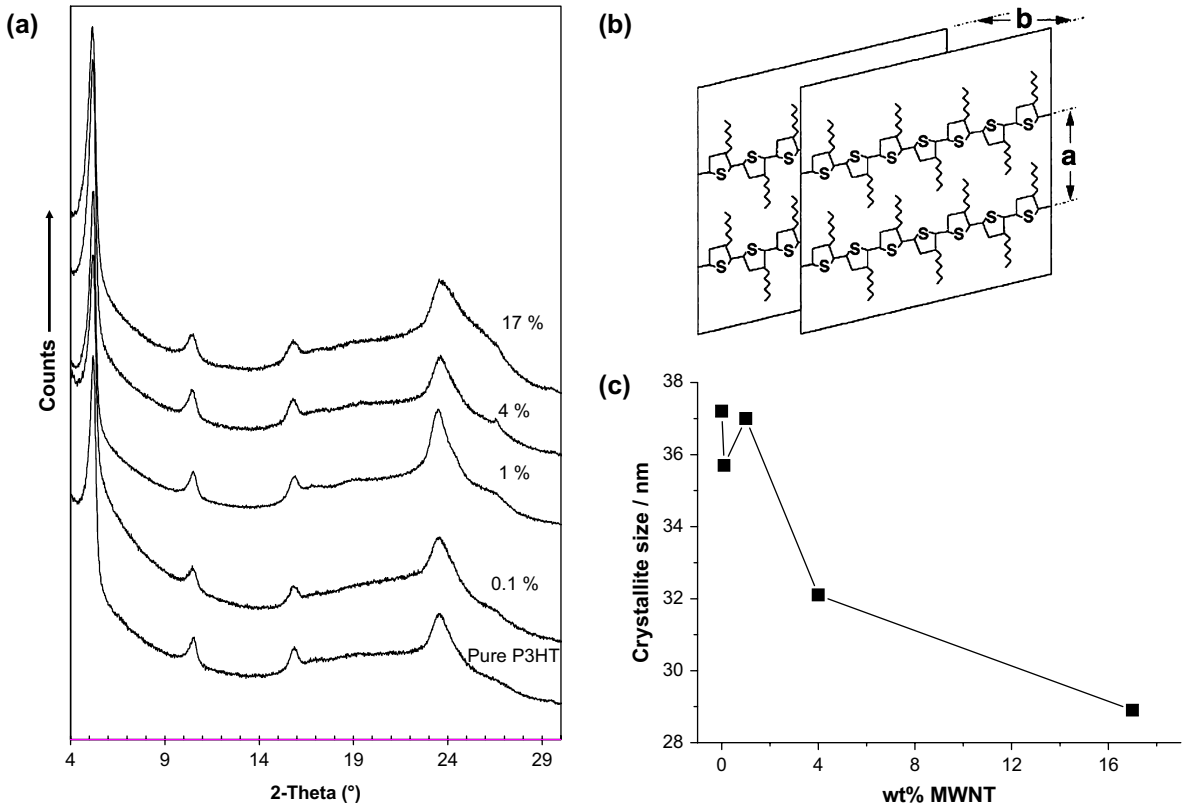

Fig. 7. (a) X-ray diffraction patterns for pure P3HT and composites obtained at room temperature, (b) lamellae structure of P3HT with interplane distance $b = 3.8$ Å and interchain distance $a = 16.8$ Å, and (c) crystallite size determined from the (100) FWHM by the Scherrer equation.

addition to an amorphous halo at wide angle, a peak with moderate intensity appears at 23.5 2θ, d-spacing 3.8 Å, which represents the stacking distance of the thiophene rings or interplane distance b.

There is no change in the scattering peaks' position with MWNT addition in the composites. However, the full-width at half-maximum (FWHM) provides some evidence for important changes occurring within the films. The FWHM for the more intense peak at 5.2° 2θ was used to calculate the crystallite size with the aid of the Scherrer equation. The results are presented in Fig. 7c. The sample with 1 wt% MWNT showed discontinuity in the general tendency of decrease in crystallite size with MWNT addition. A discontinuity in the DSC results for the maximum of melting temperature was also observed for the main peak in the case of the 1 wt% sample. Therefore, it can be affirmed that the phase organization in the composites presents two different regions before and after 1 wt% addition. After 1 wt% MWNT addition there is a decrease in polymer crystallite size and DSC transition temperature trend also indicates a decrease in long range order. It should be pointed out that despite this decrease in long range order of P3HT crystals, the conjugation length of P3HT chains, from the FTIR measurements, actually shows an increase over the range of compositions studied. Therefore, highly concentrated composites show smaller long range order but higher conformational order, which is coherent with a structure influenced by the presence of this special kind of nanofiller (MWNT) in high concentration.

3.1. Conductivity

In majority of recent studies on polymer/MWNT composites, where relatively pure NTs have been efficiently debundled and isotropically dispersed in polymer matrices, there is a convergence and increasing agreement in relation to the percolation threshold for electrical conductivity. Critical masses below 1 wt% and frequently in the order of 0.01–0.1 wt% are observed [22,25,30,32–34,36–38]. In general the efficient interaction between NT and polymer provides good dispersion and a low percolation threshold, but only relatively low conductivity near and above percolation, frequently around 10^{-4} S cm^{-1} is achieved at close to 2 wt% nanotube loading [28,33,35,38,40,41]. The polymer layer in the internanotube connections is supposed to be the highest resistance section in the electrical pathway. This polymer layer is a barrier to efficient carrier transport between NTs and models for conductivity based on fluctuation-induced tunnelling have been proposed [25].

Fig. 8 shows the results of DC conductivity as a function of temperature and MWNT loading for P3HT/MWNT. Chen and Ni [55] have reported conductivity results for pure P3AT neutral polymers. Conductivity values between 10^{-9} and 10^{-8} S cm^{-1} were observed and dependence with temperature was characterized in the range 0–200 °C. This dependence was assigned to two competitive factors: increase in electron mobility with increasing temperature and simultaneous increase in ring distortion due to α relaxation. A maximum of

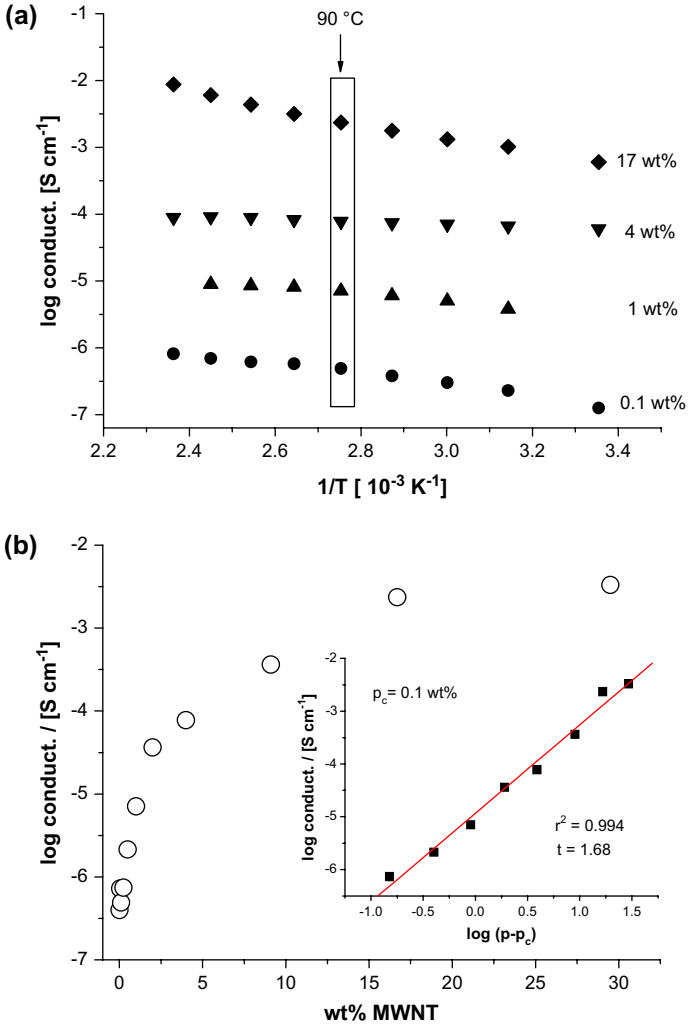

Fig. 8. Plot of the log of the conductivity (in S cm^{-1}) measured through DC-resistance technique after thermal annealing at 150 °C for 16 h: (a) as a function of inverse of temperature for typical composites with concentration shown in the figure and (b) as a function of loading of MWNTs, at 90 °C. Inset shows the linear behaviour of conductivity when plotted against $[(p-p_c)]$ with critical mass $p_c = 0.1$ wt%.

conductivity was observed at 104 °C for P3BT and 72 °C for P3OT [55]. Also, Meijer et al. [56] observed P3HT conductivity between 10^{-10} S cm^{-1} at −23 °C and 10^{-9} S cm^{-1} at 77 °C, when characterizing a diode with ITO and Au electrodes.

The results of conductivity as a function of temperature for P3HT/MWNT composites in the range 25–150 °C studied here do not show variations for the sample with 4 wt% of MWNT (Fig. 8a). An increase of conductivity with temperature was observed for the highly concentrated, 17 wt% MWNT sample, which can be associated to a mechanism of conductivity based on fluctuation-induced tunnelling [25,35] as will be discussed later. The lowest concentrated composites (0.01 and 0.05 wt%, curves not shown) exhibited a slight fluctuation of conductivity with temperature which can be related to the pure polymer conformational changes as described by Chen and Ni [55]. Besides this consideration, and also to improve contact on the electrical measurements, it was considered adequate to compare DC-conductivity measurements obtained at 90 °C for further analysis in this work.

A power law related to percolation theory can be used to model conductivity in the form

$$\sigma = \sigma_o (p - p_c)^t, \quad \text{for } p > p_c \tag{1}$$

where p_c is the critical mass or percolation threshold and the exponent t should be close to 2 for a three dimensional percolating system [35]. The results obtained from DC conductivity of P3HT/MWNT at 90 °C, as shown in inset of Fig. 8b, are $p_c = 0.1$ wt% and $t = 1.68$. These results were obtained by testing the linearity of the curve in Fig. 8b inset up to the lowest possible concentration. The value obtained for p_c compares well with several previous works where good dispersions of carbon nanotubes, both SWNT and MWNT, were obtained [1,6,25,30,33,34,36–38]. The exponent t also shows similar value to previous works [30,34–36,38]. Another fit was performed by using the percolation law as presented by McLachlan et al. [37] and the value of t changes only slightly, $t = 1.59$ in this case. The low value of t has been interpreted as associated to a fluctuation-induced tunnelling model

[25,31,34,35], where thermally induced hopping between the NTs separated by a thick polymer barrier dominates the conductivity behaviour.

To test the fluctuation-induced tunnelling model it was proposed to plot the log of DC conductivity as a function of $p^{-1/3}$, a good linear fit was considered to corroborate the approach [25,34,35]. This plot for P3HT/MWNT gives an acceptable linear behaviour for the intermediary range of compositions, between 0.25 and 10 wt% MWNT composites as observed in Fig. 9. The highly concentrated samples cannot be included in this adjustment as the quality of the linear fit decreases very rapidly. This result indicates that in the case of the highly concentrated samples a more efficient transfer of charge in the contact between tubes is achieved. This is not a surprise considering the higher level of conductivity attained with the composites in the concentrated range as can be observed in Fig. 8. Therefore, these results point to the fact that after percolation two different regimes can be characterized in the conductivity of P3HT/MWNT composites: a first regime with conductivities up to 10^{-4} S cm^{-1} and with compositions up to 10 wt%, which can be satisfactorily fitted with a tunnelling model; and a second regime where the conductivities can be raised to 10^{-2} S cm^{-1} in highly concentrated samples where the nanotubes interact closely. From our review of the literature, this scenario is quite general as it can accommodate several different experimental results [25,28–30,33,35–38].

An intriguing observation is the fact that the sample with 17 wt% of MWNT cannot be included in the region where a supposed fluctuation-induced tunnelling model would apply (Fig. 9), although, it is the sample that shows dependence of conductivity on temperature in Fig. 8a. This apparent contradictory result may be a consequence of a complex interplay of the conductivity through the carbon nanotube network assisted by transport through carbon nanotube-bridging conjugated polymer chains.

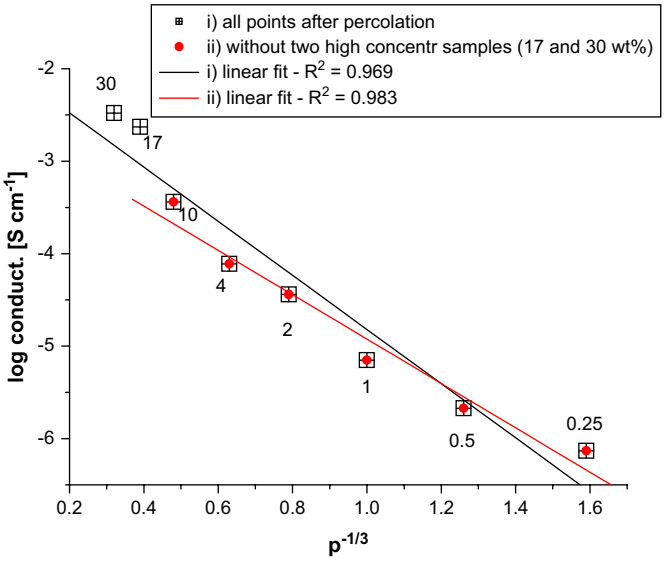

Fig. 9. Variation of log conductivity from DC results at 90 °C (in S cm^{-1}) as a function of $p^{-1/3}$ for P3HT/MWNT composites. Compositions in wt% are indicated in the figure.

Good agreement was also observed between DC and AC data. AC-impedance data for P3HT/MWNT composites are shown in Fig. 10. The highly concentrated samples displayed a frequency independent conductivity in the range of low frequency and a tendency to increase at higher frequencies. This behaviour has been observed for several systems [25,31,34,35,37] and is a matter of some debate in the literature. In our results the conductivity as a function of frequency for the diluted composites did not show the expected trend of a dielectric material. A typical dielectric should exhibit a linear increase of conductivity with frequency with a slope of unity in a log–log plot. Instead, the low frequency range presented a modulation which can be assigned to the contribution of P3HT to the total conductivity. A complete study of AC impedance will be discussed in a future publication. The contribution of P3HT to the overall conductivity in the composites is an interesting finding. There is a tendency to treat conjugated polymers and insulating polymers in a similar way within the field of polymer/carbon nanotube composites by applying percolation treatments. This is somewhat surprising considering that a conjugated polymer might be expected to facilitate

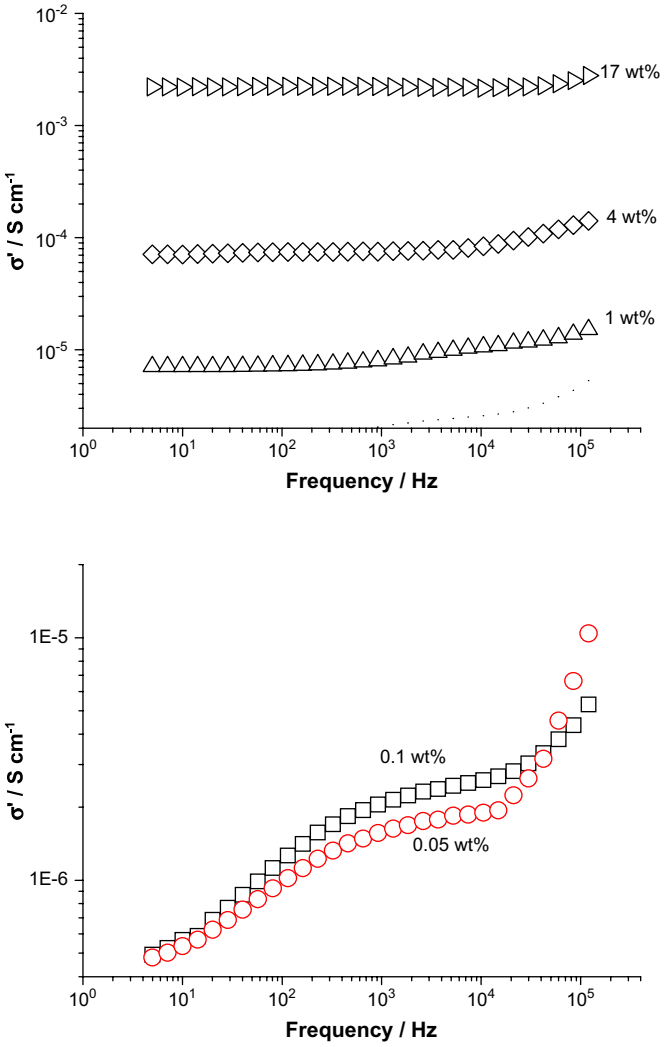

Fig. 10. Real part of AC conductivity as a function of frequency for P3HT/MWNT. Compositions are indicated in the figure.

electron transport in a composite. For some unknown reason up to now, conjugated polymer based nanocomposites have presented lower levels of conductivity than insulating polymers after percolation in some works [25,26]. It should be noted that there is a previous report of conjugated polymer contribution to the electrical and optical properties of a P3HT/MWNT composite used to prepare photovoltaic devices by Canestraro et al. [57]. Therefore, the results of AC and DC conductivities obtained here for P3HT/MWNT composites can be considered as a combination of carbon nanotube network conductivity and conjugated polymer charge transport playing different roles in different regions of MWNT concentration. For the low concentration composites, before percolation, the conductivity around 10^{-6} S cm^{-1} and frequency dependent (Fig. 10) is associated with charge transfer trough the semiconductor polymer.

The behaviour of conductivity will be discussed further by considering the information collected from SEM, TEM, FTIR, Raman, DSC and X-ray diffraction data in this work. The main conclusions of these studies can be summarized as follows: (a) a good dispersion of MWNT was achieved; (b) MWNT is efficiently wetted by P3HT; (c) conjugation length of P3HT increases with MWNT addition; (d) restriction of the C–C bond vibrations was observed on the MWNT through the polymer coating; (e) P3HT crystallinity decreases with increase in MWNT concentration after 1 wt% addition. Figs. 2–7 show a behaviour which supports the analysis of three different regions on the conductivity changes: before percolation, after percolation and up to 4 wt% and higher concentrated samples. Polymer conjugation length increases steadily with addition of 0.1 wt% MWNT and stays approximately constant for more concentrated samples. The structural studies indicate increase of long range order in the 1 wt% composite and increase of mesophase self-organization upon further nanotube addition. This trend may contribute to enhancement of composite conductivity, for example, on the effective barrier height to the electron tunnelling effect. The upshift of Raman bands for MWNT supports the conclusion that the nanotube coated with polymer is responsible for the new conductive structure of the nanocomposites.

Conductivity of an MWNT mat is reported to be approximately 10 S cm^{-1} [58], limited by the resistance of tube–tube contact. Therefore, the maximum conductivity levels expected for composites, where a polymer coating is located between NT, will depend on the type of polymer and coating thickness between tubes. The interplay of dispersion of nanotubes and contact between tubes is the central key to take full advantage of the nanometric scale of the filler. The use of self-ordered rod-like P3HT connections between tubes allowed the enhancement of charge transfer in the nanocomposite by 3 or 4 orders of magnitude when compared with other conjugated polymer/NT composites [25,26].

4. Conclusions

Self-organized rod-like P3HT superstructures were observed on the surface of MWNTs in nanocomposites. Increased polymer conjugation length and mesophase order in the bulk were identified and were associated with a carbon nanotube induced rearrangement of the P3HT chains. Bulk conductivity of P3HT/MWNT nanocomposites reached a percolation threshold of only 0.1 wt% of MWNTs. Rather than behaving as a simple insulating matrix, the conjugated polymer was observed to influence the conductivity mechanism, allowing efficient charge transfer across the internanotube connections for highly concentrated samples. The results of P3HT/MWNT study were analysed in the context of an extensive review of related reports and allowed the establishment of a general picture in the field of carbon nanotube/polymer composite materials for improvement in electrical conductivity.

Acknowledgements

G.G. Silva thanks CAPES, Brazil for grant during sabbatical year at Queensland University of Technology, Australia. E.R. Waclawik gratefully acknowledges the support of the United States' Asian Office of Aerospace Research and Development Project ID: AOARD-06-4041. The authors thank Prof. G.A. George and Prof. R.L. Frost for fruitful discussions and continuous support.

References

[1] Heeger AJ. In: Salaneck WR, Lundström I, Rånby B, editors. Proceedings of the eighty-first nobel symposium. Luleå, Sweden, 1991. Oxford University Press; 1993. p. 27–62.
[2] Shirakawa H, Louis EJ, MacDiarmid AG, Chiang CH, Heeger AJ. Journal of the Chemical Society, Chemical Communications 1977;578.
[3] Star A, Lu Y, Bradley K, Gruner G. Nano Letters 2004;4:1587–91.
[4] Yang H, Shin TJ, Yang L, Cho K, Ryu CY, Bao Z. Advanced Functional Materials 2005;15:671–6.
[5] Surin M, Leclere P, Lazzaroni R, Yuen JD, Wang G, Moses D, et al. Journal of Applied Physics 2006;100:033712-1–033712-6.
[6] Sirringhaus H, Tessler N, Friend RH. Science (Washington, D.C.) 1998; 280:1741–4.
[7] Padinger F, Rittberger RS, Sariciftci NS. Advanced Functional Materials 2003;13:85–8.
[8] Kymakis E, Koudoumas E, Franghiadakis I, Amaratunga GAJ. Journal of Physics D: Applied Physics 2006;39:1058–62.
[9] Sirringhaus H, Brown PJ, Friend RH, Nielsen MM, Bechgaard K, Langeveld-Voss BMW, et al. Nature (London) 1999;401:685–8.
[10] Kline RJ, McGehee MD, Kadnikova EN, Liu J, Frechet JMJ. Advanced Materials (Weinheim, Germany) 2003;15:1519–22.
[11] Aasmundtveit KE, Samuelsen EJ, Guldstein M, Steinsland C, Flornes O, Fagermo C, et al. Macromolecules 2000;33:3120–7.
[12] Hugger S, Thomann R, Heinzel T, Thurn-Albrecht T. Colloid and Polymer Science 2004;282:932–8.
[13] Winokur MJ, Spiegel D, Kim Y, Hotta S, Heeger AJ. Synthetic Metals 1989;28:C419–26.
[14] Tashiro K, Ono K, Minagawa Y, Kobayashi M, Kawai T, Yoshino K. Journal of Polymer Science, Part B: Polymer Physics 1991;29:1223–33.
[15] Prosa TJ, Winokur MJ, Moulton J, Smith P, Heeger AJ. Macromolecules 1992;25:4364–72.
[16] McCullough RD, Tristram-Nagle S, Williams SP, Lowe RD, Jayaraman M. Journal of the American Chemical Society 1993;115:4910–1.
[17] Ihn KJ, Moulton J, Smith P. Journal of Polymer Science, Part B: Polymer Physics 1993;31:735–42.
[18] Zhao Y, Yuan G, Roche P, Leclerc M. Polymer 1995;36:2211–4.
[19] Malik S, Nandi AK. Journal of Polymer Science, Part B: Polymer Physics 2002;40:2073–85.

[20] Trznadel M, Pron A, Zagorska M, Chrzaszcz R, Pielichowski J. Macromolecules 1998;31:5051–8.
[21] Rughooputh SDDV, Hotta S, Heeger AJ, Wudl F. Journal of Polymer Science, Part B: Polymer Physics 1987;25:1071–8.
[22] Grossiord N, Loos J, Regev O, Koning CE. Chemistry of Materials 2006; 18:1089–99.
[23] Munson-Mcgee SH. Physical Review B 1991;43:3331–6.
[24] McCarthy B, Coleman JN, Czerw R, Dalton AB, Panhuis Mih, Maiti A, et al. Journal of Physical Chemistry B 2002;106:2210–6.
[25] Kilbride BE, Coleman JN, Fraysse J, Fournet P, Cadek M, Drury A, et al. Journal of Applied Physics 2002;92:4024–30.
[26] Kymakis E, Amaratunga GAJ. Journal of Applied Physics 2006;99.
[27] Note: In considering the reported values for SWNT densities (1.4 g cm^{-3}) and typical polymer composites, the concentration in volume percent is approximately in the range 0.7–1.0 wt%. In the case of MWNT, as they have higher densities than SWNT (MW density: 1.8–2.1 g cm^{-3}), the concentration in volume percent is smaller and can be in the range 0.5–0.7 wt%.
[28] Du F, Fischer JE, Winey KI. Physical Review B: Condensed Matter and Materials Physics 2005;72:121404-1–121404-4.
[29] Koerner H, Liu W, Alexander M, Mirau P, Dowty H, Vaia RA. Polymer 2005;46:4405–20.
[30] Ramasubramaniam R, Chen J, Liu HY. Applied Physics Letters 2003;83: 2928–30.
[31] Sandler JKW, Kirk JE, Kinloch IA, Shaffer MSP, Windle AH. Polymer 2003;44:5893–9.
[32] Bryning MB, Islam MF, Kikkawa JM, Yodh AG. Advanced Materials (Weinheim, Germany) 2005;17:1186–91.
[33] Gojny FH, Wichmann MHG, Fiedler B, Kinloch IA, Bauhofer W, Windle AH, et al. Polymer 2006;47:2036–45.
[34] Kim YJ, Shin TS, Choi HD, Kwon JH, Chung YC, Yoon HG. Carbon 2005;43:23–30.
[35] Barrau S, Demont P, Peigney A, Laurent C, Lacabanne C. Macromolecules 2003;36:5187–94.
[36] Park C, Ounaies Z, Watson KA, Crooks RE, Smith J, Lowther SE, et al. Chemical Physics Letters 2002;364:303–8.
[37] McLachlan DS, Chiteme C, Park C, Wise KE, Lowther SE, Lillehei PT, et al. Journal of Polymer Science, Part B: Polymer Physics 2005;43:3273–87.
[38] Chatterjee T, Yurekli K, Hadjiev VG, Krishnamoorti R. Advanced Functional Materials 2005;15:1832–8.
[39] Zhang QH, Rastogi S, Chen DJ, Lippits D, Lemstra PJ. Carbon 2006;44: 778–85.
[40] McNally T, Potschke P, Halley P, Murphy M, Martin D, Bell SEJ, et al. Polymer 2005;46:8222–32.
[41] Potschke P, Dudkin SM, Alig I. Polymer 2003;44:5023–30.
[42] Du FM, Fischer JE, Winey KI. Journal of Polymer Science, Part B: Polymer Physics 2003;41:3333–8.
[43] Du FM, Scogna RC, Zhou W, Brand S, Fischer JE, Winey KI. Macromolecules 2004;37:9048–55.
[44] Mena-Osteritz E, Meyer A, Langeveld-Voss BMW, Janssen RAJ, Meijer EW, Bauerle P. Angewandte Chemie International Edition 2000;39:2680–4.
[45] Mena-Osteritz E. Advanced Materials 2002;14:609–16.
[46] Scifo L, Dubois M, Brun M, Rannou P, Latil S, Rubio A, et al. Nano Letters 2006;6:1711–8.
[47] Furukawa Y, Akimoto M, Harada I. Synthetic Metals 1987;18:151–6.
[48] Baskaran D, Mays JW, Bratcher MS. Chemistry of Materials 2005;17: 3389–97.
[49] Osterbacka R, An CP, Jiang XM, Vardeny ZV. Synthetic Metals 2001; 116:317–20.
[50] Wise KE, Park C, Siochi EJ, Harrison JS. Chemical Physics Letters 2004; 391:207–11.
[51] Prosa TJ, Winokur MJ, McCullough RD. Macromolecules 1996;29: 3654–6.
[52] Causin V, Marega C, Marigo A, Valentini L, Kenny JM. Macromolecules 2005;38:409–15.
[53] Kuila BK, Nandi AK. Macromolecules 2004;37:8577–84.
[54] Ryan KP, Lipson SM, Drury A, Cadek M, Ruether M, O'Flaherty SM, et al. Chemical Physics Letters 2004;391:329–33.
[55] Chen SA, Ni JM. Macromolecules 1992;25:6081–9.
[56] Meijer EJ, Mangnus AVG, Hart CM, de Leeuw DM, Klapwijk TM. Applied Physics Letters 2001;78:3902–4.
[57] Canestraro CD, Schnitzler MC, Zarbin AJG, da Luz MGE, Roman LS. Applied Surface Science 2006;252:5575–8.
[58] de Heer WA, Bacsa WS, Chatelain A, Gerfin T, Humphrey-Baker R, Forro L, et al. Science 1995;268:845–7.